ACS OMEGA

http://pubs.acs.org/journal/acsodf

Article

Interfacial Oxidized Gate Insulators for Low-Power Oxide Thin-Film Transistors

In Hye Kang, Sang Ho Hwang, Young Jo Baek, Seo Gwon Kim, Ye Lin Han, Min Su Kang, Jae Geun Woo, Jong Mo Lee, Eun Seong Yu, and Byung Seong Bae*

Cite This: *ACS Omega* 2021, 6, 2717−2726

Read Online

ACCESS | Metrics & More | Article Recommendations

ABSTRACT: Low power consumption is essential for wearable and internet-of-things applications. An effective way of reducing power consumption is to reduce the operation voltage using a very thin and high-dielectric gate insulator. In an oxide thin-film transistor (TFT), the channel layer is an oxide material in which oxygen reacts with metal to form a thin insulator layer. The interfacial oxidation between the gate metal and In−Ga−Zn oxide (IGZO) was investigated with Al, Ti, and Mo. Positive bias was applied to the gate metal for enhanced oxygen diffusion since the migration of oxygen is an important factor in interfacial oxidation. Through interfacial oxidation, a top-gate oxide TFT was developed with low source−drain voltages below 0.5 V and a gate voltage swing less than 1 V, which provide low power consumption.

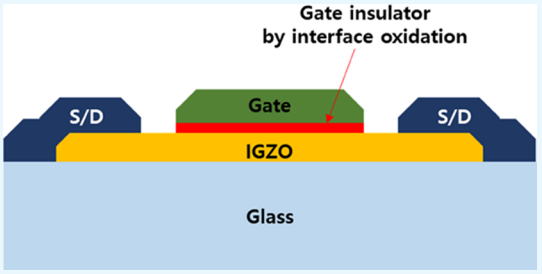

INTRODUCTION

Thin-film transistors (TFTs) are core devices in display backplanes and are being studied for applications such as wearable and stretchable displays.[1−7] Recently, amorphous In−Ga−Zn oxide (a-IGZO) TFTs were applied to the backplanes of organic light-emitting diode (OLED) televisions due to their large-area processability and larger electron mobility than that of amorphous silicon TFTs. For extended applications, low power consumption is necessary, and the reduction of the operation voltage is essential because the power is inversely proportional to the square of the operation voltage.[8,9]

The induced areal charge density in the channel of a TFT is proportional to the gate dielectric capacitance per unit area, which is ε/t, where ε and t are the permittivity and thickness of the gate dielectric, respectively. Thus, an effective way to decrease the operating voltage of a TFT is reducing the thickness of the gate insulator.

The usual ways of depositing a gate dielectric are vacuum processes such as plasma-enhanced chemical vapor deposition (PECVD), sputtering, and atomic layer deposition (ALD).[10,11] The deposition of a thin gate dielectric is one way to decrease the operating voltage of a TFT.[12−17] For a thin high-dielectric gate insulator, aluminum anodic oxidation was applied to obtain an IGZO TFT with a 1 V operation voltage.[14,18−28]

For the gate insulator, we used the interfacial reaction between an oxide semiconductor and gate metal instead of a vacuum-deposited insulator. The formation of metal oxide by the reaction between metal and oxide has been reported in devices such as a-IGZO TFTs and resistive switching memory.[29−33] The source/drain contact in an IGZO TFT is quite different from a silicon active layer, which has no oxygen. The reaction between the source/drain metal and IGZO has been reported. In the IGZO layer, oxygen bonds to metal ions or exists as interstitial oxygen, and the reaction with the source/drain metal results in thin metal oxide, which increases the contact resistance. Usually, thermal annealing accelerates the formation of the metal oxide, and annealing effects have been reported for various metals. The interfacial oxide between the source/drain and active oxide layer in a-IGZO TFTs degrades the device performance due to the high contact resistance.

For some metals with high oxygen affinity, such as Al, a thin metal oxide region of a few nanometers is observed just after sputter deposition, even without thermal annealing. The increased source/drain contact resistance from the metal oxide deteriorates the characteristics of a TFT, so metals that have low oxygen affinity are preferable to avoid high source/drain contact resistance.[30,34−41] However, in this study, we developed interfacial oxide that is applicable to a gate insulator that is very thin to obtain a low threshold voltage. For a more stable insulator, we used metals that have a great tendency to oxidize based on the Gibbs free energies. One advantage of the interfacial oxidation is the use of a plasma-free process that

Received: October 8, 2020
Accepted: January 6, 2021
Published: January 15, 2021

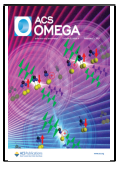

prevents plasma-induced defects in a-IGZO, which deteriorates the performance of the TFT.

However, the metal oxide from migrating oxygen is too thin to be used as a gate insulator. To obtain a reliable insulator for low-operation-voltage TFT, the diffusion of interstitial oxygen or oxygen that was broken from the metal in IGZO plays an important role. The substrate is a glass, so the diffusion of the oxygen at a low temperature below 400 °C is essential.[42,43] The oxidation can be enhanced by an electric field, which is known as anodic oxidation. In anodic oxidation, a positive voltage is applied to the metal to enhance the oxidation, and the anodic oxidation under an electrolyte is widely used to form an oxide layer at room temperature. The electrolyte anodization of Al was applied for the channel passivation of IGZO TFT, and the change in the oxygen and metal atomic concentrations was observed under an electric field in an all-solid system such as an IGZO film.[44,45]

METHODS

Figure 1 shows a cross-sectional structure of the top-gate a-IGZO TFT developed in this study. A 50 nm IGZO layer was deposited on glass by RF sputtering with an IGZO target under Ar/O_2 gas with a ratio of 22.5/7.5 sccm. After applying an IGZO active pattern by photolithography, thermal annealing was done at 250 °C under an oxygen atmosphere.

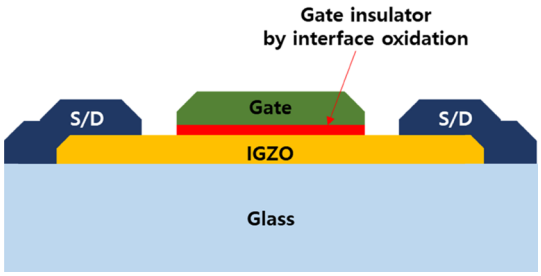

Figure 1. Top-gate a-IGZO TFT with a gate insulator by interfacial oxidation.

Gate metal was sputtered on the IGZO layer and patterned for the gate electrode by photolithography. The gate electrode contacts the IGZO, and the interfacial oxidation occurs during the furnace annealing. The annealing temperature and time were controlled to find the optimum conditions. The source and drain regions were doped by oxygen plasma treatment, which decreases the resistance of the a-IGZO layer between the channel and source/drain electrodes. Finally, source/drain metal was formed by wet etching after deposition of the metal by DC sputtering.

To evaluate the interfacial oxidation, samples were prepared with a sandwich structure of metal (0.8 mm diameter)/a-IGZO/ITO (indium tin oxide)/glass. After furnace annealing for the interfacial oxidation between the metal and IGZO, the current−voltage ($I-V$) characteristics were measured to investigate the leakage currents and breakdown voltages. Ti, Mo, and Al were studied for interface oxidation.

RESULTS AND DISCUSSION

$I-V$ characteristics were investigated after interfacial oxidation annealing at 400 °C for 1.5 h under an air atmosphere. Figure 2a shows the $I-V$ characteristics at several measurement points on the sample with Al metal electrodes. Some curves show breakdown voltages around 0.4 and 0.6 V, while some curves show very low breakdown voltage around zero because of particles or pinholes. For the Mo electrode shown in Figure 2b, the breakdown voltage is about 0.08 V, which is lower than that of the Al electrode. For the Ti electrode, the breakdown voltage is also low at 0.09 V, as shown in Figure 2c. Among the three metals, the Al electrode has the highest breakdown voltage.

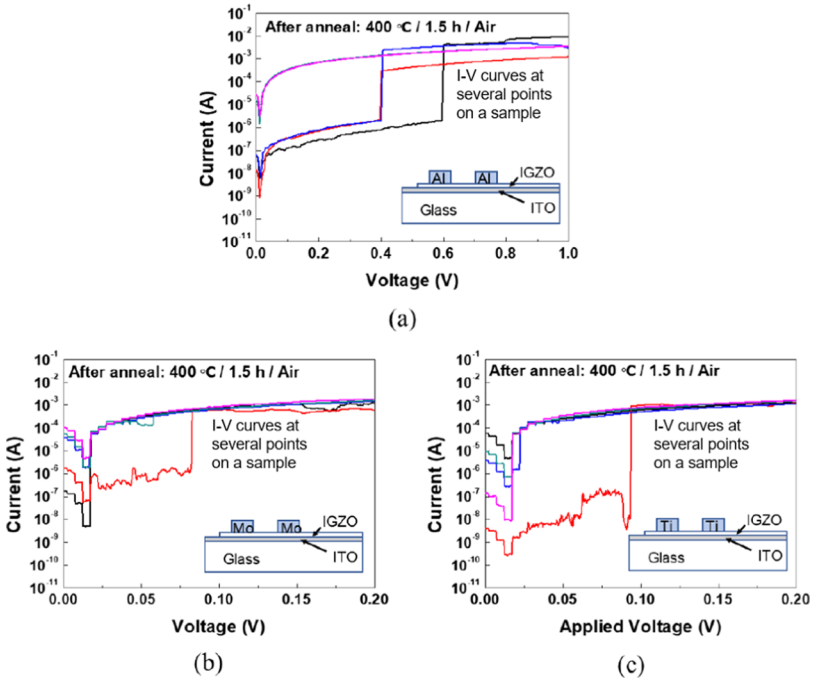

Figure 2. $I-V$ characteristics after interfacial oxidation by furnace annealing at 400 °C for 1.5 h under an air atmosphere with various metal electrodes Al (a), Mo (b), and Ti (c).

https://dx.doi.org/10.1021/acsomega.0c04924
ACS Omega 2021, 6, 2717−2726

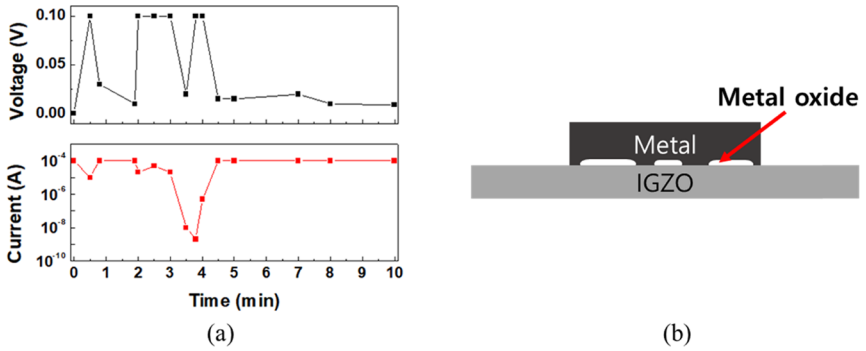

Figure 3. (a) Fluctuation of anodic currents and voltages during anodic oxidation and the (b) proposed anodic oxidation model.

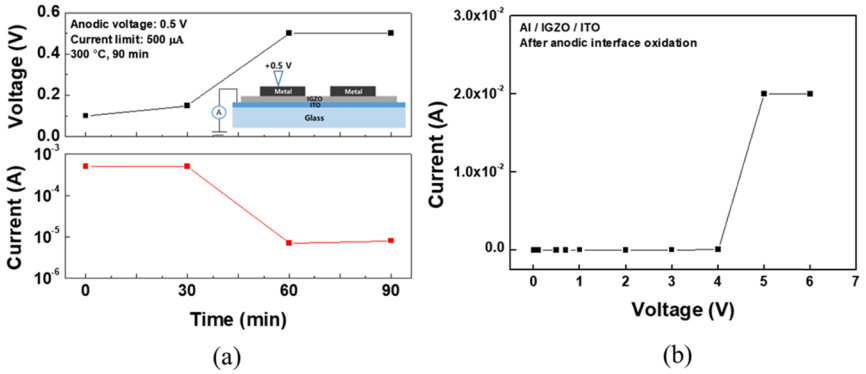

Figure 4. (a) Anodic voltage and current during anodic oxidation after the thermal interfacial oxidation process and (b) *I*–*V* characteristics of anodic oxidized metal oxide.

Interfacial oxidation occurs at the interface between metal and an IGZO layer and forms a very thin metal oxide layer. Oxygen bonds to the metal cations at the metal–IGZO interface or interstitial oxygen diffuses to the gate metal to form metal oxide. The reactivity depends on the kind of metal, and metal with lower Gibbs free energy has higher oxygen affinity. The Gibbs free energies of formation (ΔG_f) for Al_2O_3, TiO_2, and MoO_2 are −1582.3, −888.8, and −533.0 kJ/mol, respectively.[46] Al_2O_3 has the lowest ΔG_f, which explains the highest breakdown voltage of the interfacial oxide with Al. Due to its quite low Gibbs free energy, aluminum forms metal oxide quickly when contacting the oxide materials. Aluminum oxide was reported at the interface of aluminum deposited on an IGZO layer, even without thermal annealing.

The breakdown voltages of the interfacial oxidized insulator of the Al electrode are low (around 0.4–0.6 V), as shown in Figure 2a. However, to obtain a TFT operation voltage of 0.5 V, the breakdown voltage should be more than 0.5 V. To improve the breakdown voltage of the interfacial oxidized insulator, we performed anodic oxidation in air by applying a positive voltage to the metal electrode. The oxidation of the metal requires oxygen, which should reach the metal surface, so the diffusion of oxygen ions from IGZO to the metal is essential. This can be accelerated by anodic oxidation. The effects of electric fields are not well understood; however, an applied electric field enhances the oxygen diffusion and forms the metal oxide easily. During anodic oxidation, first oxidation occurs by a charge transport-mediated oxidation–reduction process. Further oxidation of the metal needs the oxygen atoms to diffuse across the metal oxide from the oxygen source. Many oxides with ionic bonding characters are known to show ionic conduction and the oxygen diffusion is enhanced by the electric field.[47−49]

After setting the compliance current at 50 μA, we applied 0.1 V to the metal electrode at a substrate temperature of 250 °C. During the anodic oxidation, we monitored the anodic voltages and currents, as shown in Figure 3a. When the anodic oxidation proceeded, the anodic current decreased and the anodic voltage approached the set voltage. However, after a decrease of the anodic current by oxidation, a sudden increase of the anodic current occurred repeatedly, which is explained by the model shown in Figure 3b.

Before oxidation of the whole area, there are regions not covered by anodic oxide, which can be paths for the anodic current. Therefore, there is a relatively long incubation time before the fast decrease of the anodic current. When the whole area is covered by anodic oxide, the anodic currents decrease rapidly, and then the electric breakdown of the weakly bonded area occurs, which increases the anodic current again. The experimental results show that anodic oxidation and electric breakdown occurred irregularly, as shown in Figure 3a.[50]

The fluctuation of the anodic currents was resolved by preannealing. Before anodic oxidation, thermal interfacial oxidation was performed by furnace annealing at 300 °C for 1 h. Preannealing improved the anodic oxidation process without fluctuation of the anodic currents, as shown in Figure 4a. The anodic oxidation process occurred after a specific incubation time because the current path is still open until the whole surface area becomes oxidized and blocks the current pathway. The change in the current with the anodizing time can be divided into two distinct parts: (1) the formation of a metal oxide barrier that blocks all of the leakage paths and results in a rapid drop of the anodic current; and (2) the

https://dx.doi.org/10.1021/acsomega.0c04924
ACS Omega 2021, 6, 2717−2726

steady-state growth of metal oxide after the metal oxide barrier.[51−53]

After anodic oxidation, the breakdown voltage increased remarkably compared to the interfacial oxide from furnace annealing only. The measured breakdown voltages for the anodic interfacial oxide were higher than 4 V, as shown in Figure 4b. Assuming a dielectric strength of 6 MV/cm, the estimated thickness from the breakdown voltage is in the range of 7−8 nm. The anodic oxidation was tested repeatedly, and the breakdown voltage distribution was rather broad. For reproducible results, more research on the interfacial oxidation is required. Many variables can affect the interfacial oxidation, such as the annealing temperature, the anodic temperature, voltage, and current.

The change of the anodic voltage and current during anodic oxidation is shown in Figure 5 for a nonannealed sample after

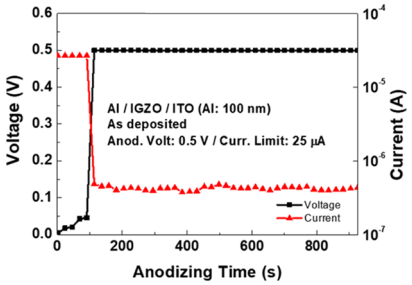

Figure 5. Anodic voltage and currents during the anodic interfacial oxidation without annealing after metal electrode deposition.

the deposition of Al on IGZO. Due to the current limit of 25 μA, the anodic voltage was low at first (below 0.1 V). The anodic voltage increased over time, reached the applied bias of 0.5 V, and switched to a constant-voltage mode. The decreased current is due to the formation of metal oxide at the metal interface with the IGZO layer.[54,55] The $I-V$ characteristics were measured and are shown in Figure 6a.

The leakage currents increased when increasing the voltages, and finally, the breakdown occurred at 1.65 V. The low leakage current and breakdown at 1.65 V verify the formation of the metal oxide between the metal and IGZO by anodic oxidation. The $I-V$ characteristics without anodic oxidation are shown in Figure 6b. The currents are high compared to those of the anodically oxidized sample, which proves the importance of anodic oxidation to obtain an excellent insulator with low leakage current.

The thermal annealing before anodic oxidation improves the characteristics of the anodic oxide due to the thin interfacial metal oxide. Thin thermal oxide can promote uniform oxidation at the interface and the weak point can be decreased after anodic oxidation. The anodic currents and voltages for the samples with thermal annealing are shown in Figure 7a,b. Figure 7a shows the anodic currents and voltages for the samples annealed at 200 °C for 1 h in air. The anodic currents decrease after some incubation time, and the anodic voltage increases due to the formation of the anodic oxide. Figure 7b shows the anodic currents and voltages for the sample annealed at 300 °C for 1 h in air. After an incubation time of ∼3000 s, the anodic current decreased due to the formation of the anodic oxide.

The $I-V$ characteristics for the sample anodically oxidized after annealing at 300 °C are shown in Figure 8. The breakdown voltage improved to 2.95 V compared to 1.65 V for the sample anodically oxidized without thermal annealing, as shown in Figure 6a. The leakage currents are also improved for the annealed sample before anodic oxidation.

High-resolution transmission electron microscopy (HRTEM) images were observed for the samples annealed at 300 °C for 1 h under ambient conditions. Figure 9a,b shows the HRTEM images for both samples before anodic oxidation and after anodic oxidation. Without anodic oxidation, the interface between the Al and IGZO is blurry and not clear. However, with anodization after annealing, the aluminum oxide region can be seen more clearly, and the thickness of the interfacial region is about 8 nm. Therefore, the breakdown voltage improvement after anodic oxidation is due to the denser and more uniform aluminum oxide.

Figure 10 shows the energy-dispersive X-ray distribution spectroscopy (EDS) results as a function of depth. Figure 10a shows the sample without anodization after thermal annealing at 300 °C for 1 h, and Figure 10b shows the sample with anodization after thermal annealing. The electric field enhances the oxygen ion diffusion during anodic oxidation by the positive voltage on the metal, so the oxygen diffuses to a longer distance. The oxygen distribution at the interface between Al and IGZO is also broader than that of the sample without anodization, as shown in Figure 10b. Oxygen travels far more distance from the In-rich region than that of the sample without anodization due to the enhanced mobility of the oxygen ions by the electric field.

Figure 11a shows the X-ray photoelectron spectroscopy (XPS) spectrum of Al 2p at the surface of the Al and inside the Al film. The binding energies of Al metal and Al oxide are 72.6

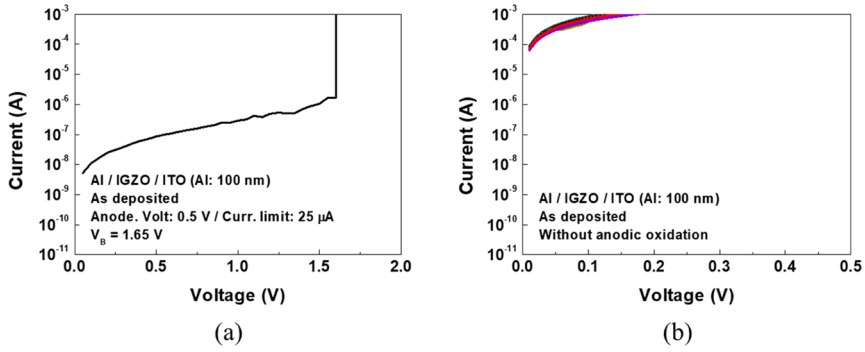

Figure 6. $I-V$ characteristics for the sample (a) with anodic oxidation and (b) without anodic oxidation.

https://dx.doi.org/10.1021/acsomega.0c04924
ACS Omega 2021, 6, 2717−2726

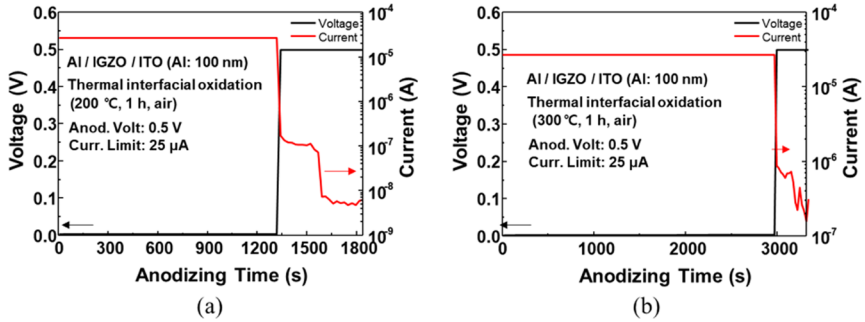

Figure 7. Anodic currents and voltages for the samples annealed at 200 °C (a) and 300 °C (b).

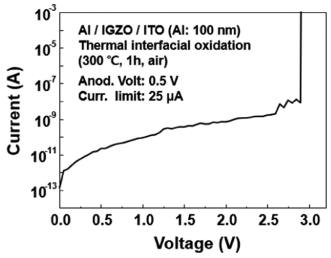

Figure 8. *I*−*V* characteristics of the sample annealed at 300 °C before anodic oxidation.

and 74.6 eV, respectively. The sample structure is Al/IGZO/ITO/glass.

The surface of Al is oxidized and the Al 2p 74.6 eV peak is dominant; meanwhile, the 72.6 eV peak is dominant inside Al. To clarify the interface between Al and IGZO layer, the depth profile for the 74.6 eV was drawn, as shown in Figure 11b. The Al 2p 74.6 eV peak is increased as it approaches the interface with IGZO, which indicates the aluminum oxide at the interface.

Interfacial oxidation of the metal that contacts the IGZO layer is essential for stable operation of the TFT without breakdown during operation. The interfacial oxidation by thermal annealing cannot easily obtain a satisfactory insulator for a-IGZO TFTs, so anodic oxidation after thermal annealing was applied to the interface between the gate metal and IGZO layer. Anodic oxidation was done after the completion of the full process of the top-gate-structure TFT shown in Figure 1. The source and drain electrodes were connected to the ground, and a positive voltage of 10 V was applied to the gate electrode with a 10 μA current limit, while the substrate temperature was kept at 380 °C. As the oxidation proceeded, the anodic currents decreased, as shown in Figure 12.

An advantage of anodic oxidation is the ability to monitor the oxidation process by the anodic current because the anodic current decreases as the anodic oxide is formed. That is, we can check the formation of the gate insulator. Different from the previous anodic oxidation voltages, a definite change of anodic voltages was not observed in the TFT structure, as shown in Figure 12. We suggest that the reason is the relatively high resistance of the source/drain offset region, which acts as a series resistance for the anodic oxidation currents.

After cooling to room temperature, the transfer and output characteristics were measured after oxygen annealing. Before the electrical measurement, we tested whether the contact to the metal pad had no problem because the surface oxidation of the metal pad can resist the current flow. A pad was contacted with two probe tips to check the current−voltage characteristics. If the currents were very low, the contact was adjusted to assure low contact resistance on the pad. After that, one of the probe tips was removed and the TFT characteristics were measured. The W/L of the TFT was 25/10, and the transfer curves and output curves are shown in Figure 13a,b.

The currents at V_{DS} = 0 V are leakage currents through the gate insulator and are very low compared to the drain currents. This shows that the drain currents are not leakage currents through the gate insulator. During interfacial oxidation, the interstitial oxygen moves to the metal surface, and a few oxygen bonds near the metal interface are broken to migrate to

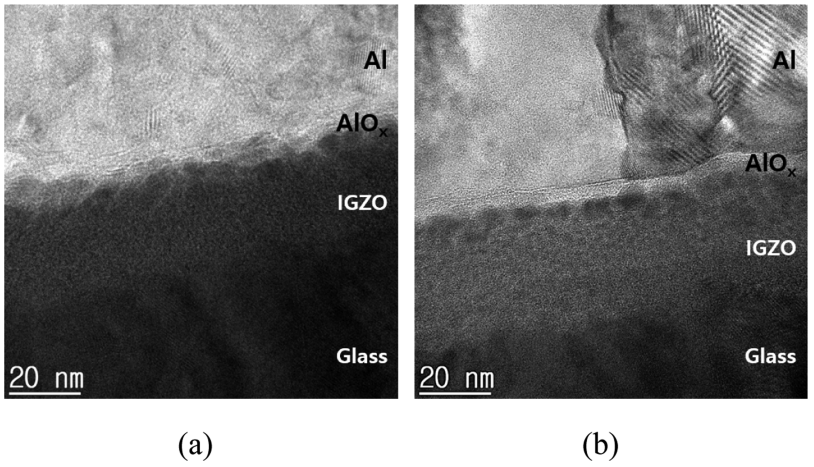

Figure 9. HRTEM of the interface between Al and IGZO (a) without anodic oxidation and (b) with anodic oxidation.

https://dx.doi.org/10.1021/acsomega.0c04924
ACS Omega 2021, 6, 2717−2726

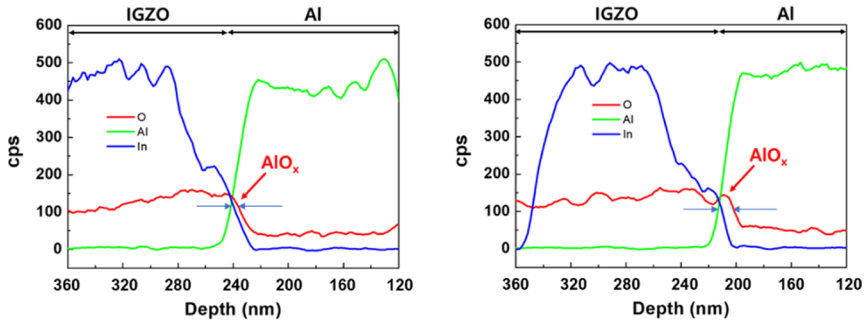

Figure 10. EDS analysis as a function of depth (a) without anodic oxidation and (b) with anodic oxidation. For the sample with anodic oxidation, the oxygen distribution is farther from the In-rich region than that of the sample without anodic oxidation.

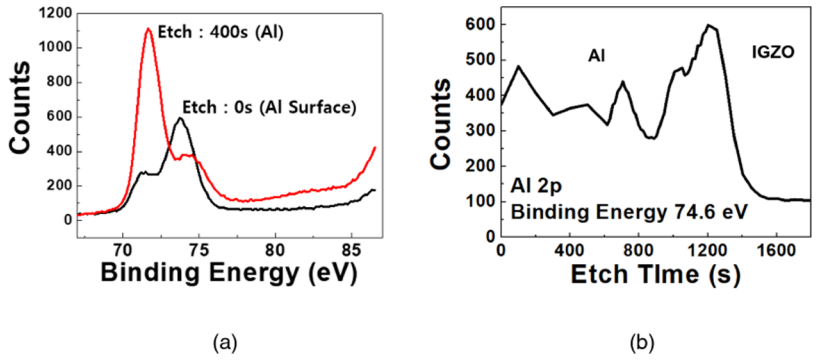

Figure 11. (a) Binding energy spectra of Al 2p at the surface and inside of the Al and the (b) depth profile of Al 2p of binding energy 74.6 eV.

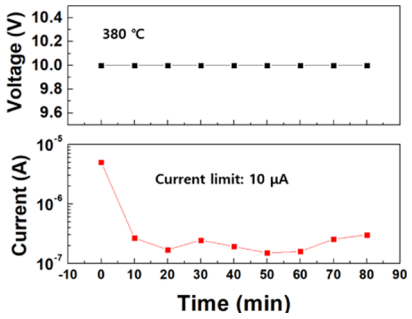

Figure 12. Anodic voltages and currents during anodic oxidation after the completion of the IGZO TFT.

the metal surface. The removal of the lattice oxygen bonded to the metal cation causes an increase of the oxygen vacancies, which increase the carrier density in the conduction band of the a-IGZO.

The increased channel conductivity by the increase of the carrier concentration results in a negative shift of the threshold voltage, as shown in Figure 13a. A low operation voltage V_{DS} below 0.5 V and a voltage V_{GS} swing less than 1 V were achieved for the top-gate a-IGZO TFT with a very thin interfacial oxidized gate insulator. The threshold voltage, subthreshold swing, and on−off ratio were −1.3 V, 0.1 V/dec, and 4.9×10^5, respectively.

However, the very low on-current is a problem to be solved and is under development to be increased. One reason that we suggest is increased oxygen vacancies related to a negative shift of the threshold voltage, which increases the scattering of the carriers and reduces the mobility. Another reason could be the large source/drain contact resistance, which can be seen in the

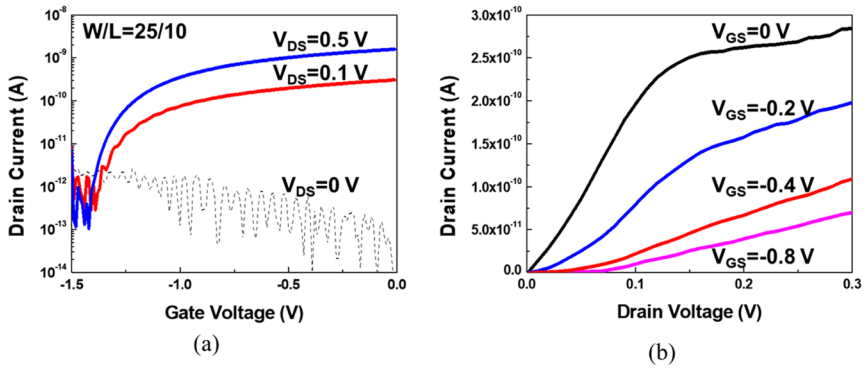

Figure 13. Transfer characteristics of the developed interfacial oxidized gate insulator oxide TFT (a) and output characteristics (b).

https://dx.doi.org/10.1021/acsomega.0c04924
ACS Omega 2021, 6, 2717−2726

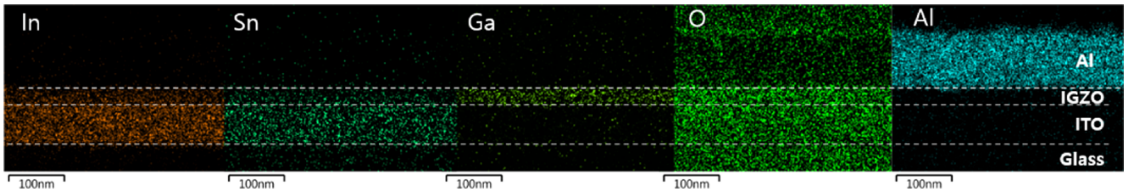

Figure 14. EDS mapping of the Al/IGZO/ITO/glass sample after 300 °C annealing.

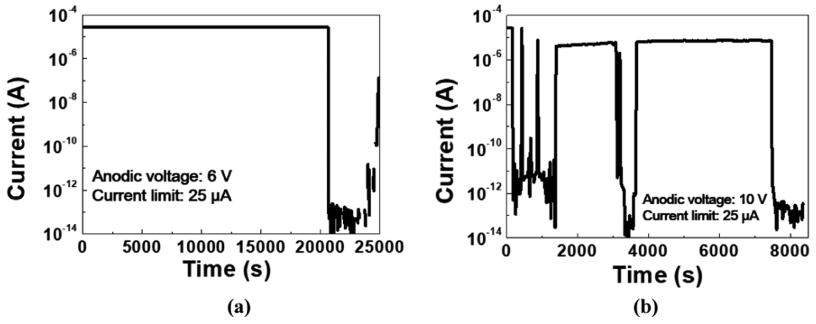

Figure 15. Anodic current variations during anodic oxidation with anodic voltages of 6 V (a) and 10 V (b).

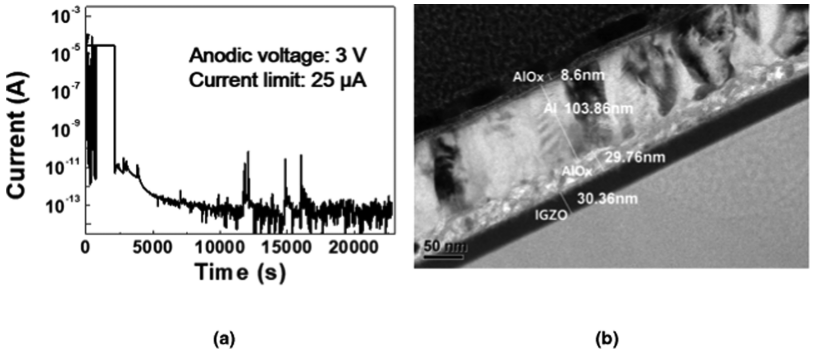

Figure 16. Anodic currents during anodic oxidation of the sample Al/IGZO/Si wafer (a) and the high-resolution transmission electron microscopy (HRTEM) image at the interface after interfacial oxidation (b).

current crowding at low drain voltages, as shown in Figure 13b. The large contact resistance increases the voltage drop at the contact region, so the decreased lateral electric field by the parasitic contact resistance results in the reduction of on-currents. The IGZO could also be defective from energetic ions during the gate metal deposition by sputtering, which deteriorates the TFT characteristics significantly. Therefore, the deposition conditions of the gate metal are also important for high on-current.

The effects of Al diffusion into the IGZO are reported that Al acts as a carrier suppressor, which reduces the conductivity.[56] Figure 14 shows the EDS mapping data after 300 °C annealing of the Al/IGZO/ITO sample.

Much oxygen was distributed along whole layers except Al. Sn is abundant in IGZO, which shows much diffusion of Sn into the IGZO. In terms of Al, a little distribution of Al is observed in IGZO and ITO. The Al atoms observed in the IGZO layer can act as a carrier suppressor, which deteriorate the device performance.

We used anodic oxidation for the interfacial oxidation for the gate insulator. The anodic oxidation shows several cases and needs further research. Figure 15a,b shows typical abnormal fluctuation of anodic currents during anodic oxidation. The process was irregular and needed optimum conditions of the oxidation.

Figure 16a shows standard anodic current during anodic oxidation for the sample to get a dielectric constant of the insulator. The sample structure was Al/IGZO/Si wafer to measure the capacitance of the anodic oxide. On a doped silicon wafer, an IGZO layer was deposited and then an Al electrode of 1.0 mm diameter was deposited using a shadow mask. Before interfacial oxidation, we measured capacitance and then annealed at 400 °C for 4 h under an oxygen atmosphere followed by anodic oxidation. The anodic currents during anodic oxidation are shown in Figure 16a. The anodic voltage and current limit were 3 V and 25 μA, respectively. After anodic oxidation, we measured the capacitance again to get the capacitance of the anodic oxide.

Since the interfacial oxide forms the series-connected capacitance, we obtained the capacitance of the interfacial oxide from the equation of the total capacitance C of two series-connected capacitors as (C1 and C2) $1/C = 1/C1 + 1/C2$. Figure 16b shows the HRTEM image at the interface after anodic oxidation to obtain the thickness of the oxide. We assume that the oxide thickness before oxidation is 4 nm. The measured capacitances before and after interfacial oxidation were 172 and 188 pF, respectively. The calculated dielectric constant was 7.5, which is rather lower than the dielectric constant of Al_2O_3, which was attributed to the nonstoichiometric structure of the aluminum oxide.

https://dx.doi.org/10.1021/acsomega.0c04924
ACS Omega 2021, 6, 2717−2726

CONCLUSIONS

The interfacial oxidation between metal and an IGZO layer was investigated by thermal annealing and anodic oxidation. Metal oxide suitable for the gate insulator of a low-operation-voltage IGZO TFT was obtained by anodic oxidation after thermal annealing. Al, Ti, and Mo were investigated, and Al was the most suitable for the interfacial oxidation for the gate insulator. Based on the experiments, a top-gate IGZO TFT was successfully developed with a gate insulator by interfacial oxidation. The threshold voltage, subthreshold swing, and on−off ratio were −1.3 V, 0.1 V/dec, and 4.9×10^5, respectively. The developed device provides low operation voltages below 0.5 V and the voltage swing less than 1 V for low power consumption. The low on-currents should be resolved. The suggested reasons for the low on-currents were vacancies generated during the oxidation, high contact resistance, diffused Al atoms into the IGZO, and bombardment of energetic ions during the gate metal deposition by sputtering. Further research is being done to improve the on-current.

AUTHOR INFORMATION

Corresponding Author

Byung Seong Bae − *School of Electronics and Display Engineering, Hoseo University, Asan, Chungnam 31499, Korea;* orcid.org/0000-0002-3328-0286; Email: bsbae3@hoseo.edu

Authors

In Hye Kang − *School of Electronics and Display Engineering, Hoseo University, Asan, Chungnam 31499, Korea*

Sang Ho Hwang − *School of Electronics and Display Engineering, Hoseo University, Asan, Chungnam 31499, Korea*

Young Jo Baek − *School of Electronics and Display Engineering, Hoseo University, Asan, Chungnam 31499, Korea*

Seo Gwon Kim − *School of Electronics and Display Engineering, Hoseo University, Asan, Chungnam 31499, Korea*

Ye Lin Han − *Department of NanoBioTronics, Hoseo University, Asan, Chungnam 31499, Korea*

Min Su Kang − *School of Electronics and Display Engineering, Hoseo University, Asan, Chungnam 31499, Korea*

Jae Geun Woo − *School of Electronics and Display Engineering, Hoseo University, Asan, Chungnam 31499, Korea*

Jong Mo Lee − *School of Electronics and Display Engineering, Hoseo University, Asan, Chungnam 31499, Korea*

Eun Seong Yu − *School of Electronics and Display Engineering, Hoseo University, Asan, Chungnam 31499, Korea*

Complete contact information is available at: https://pubs.acs.org/10.1021/acsomega.0c04924

Funding

Authors In Hye Kang, Seo Gwon Kim, Min Su Kang, and Byung Seong Bae received funding from National Research Foundation of Korea (NRF), Grant number 2017R1D1A1A02019514.

Notes

The authors declare no competing financial interest.

ACKNOWLEDGMENTS

This research was supported by the Basic Science Research Program through the National Research Foundation of Korea (NRF), which is funded by the Ministry of Education (2017R1D1A1A02019514).

ABBREVIATIONS

TFT, thin-film transistor; a-IGZO, amorphous In−Ga−Zn oxide; OLED, organic light-emitting diode; PECVD, plasma-enhanced chemical vapor deposition; ALD, atomic layer deposition; ITO, indium tin oxide; *I*−*V*, current−voltage; HRTEM, high-resolution transmission electron microscope; EDS, energy-dispersive X-ray distribution spectroscopy; XPS, X-ray photoelectron spectroscopy

REFERENCES

(1) Someya, T.; Kato, Y.; Sekitani, T.; Iba, S.; Noguchi, Y.; Murase, Y.; Kawaguchi, H.; Sakurai, T. Conformable, flexible, large-area networks of pressure and thermal sensors with organic transistor active matrixes. *Proc. Natl. Acad. Sci.* **2005**, *102*, 12321−12325.

(2) Rim, Y. S.; Bae, S. H.; Chen, H.; De Marco, N.; Yang, Y. Recent progress in materials and devices toward printable and flexible sensors. *Adv. Mater.* **2016**, *28*, 4415−4440.

(3) Nomura, K.; Ohta, H.; Takagi, A.; Kamiya, T.; Hirano, M.; Hosono, H. Room-temperature fabrication of transparent flexible thin-film transistors using amorphous oxide semiconductors. *Nature* **2004**, *432*, 488−492.

(4) Kim, Y.-G.; Tak, Y. J.; Kim, H. J.; Kim, W.-G.; Yoo, H.; Kim, H. J. Facile fabrication of wire-type indium gallium zinc oxide thin-film transistors applicable to ultrasensitive flexible sensors. *Sci. Rep.* **2018**, *8*, No. 5546.

(5) Wang, S.; Xu, J.; Wang, W.; Wang, G.-J. N.; Rastak, R.; Molina-Lopez, F.; Chung, J. W.; Niu, S.; Feig, V. R.; Lopez, J.; et al. Skin electronics from scalable fabrication of an intrinsically stretchable transistor array. *Nature* **2018**, *555*, 83−88.

(6) Chortos, A.; Bao, Z. Skin-inspired electronic devices. *Mater. Today* **2014**, *17*, 321−331.

(7) Zhou, L.; Wanga, A.; Wu, S.-C.; Sun, J.; Park, S.; Jackson, T. N. All-organic active matrix flexible display. *Appl. Phys. Lett.* **2006**, *88*, No. 083502.

(8) Hosticka, B. J.; Brockherde, W.; Hammerschmidt, D.; Kokozinski, R. Low-voltage CMOS analog circuits. *IEEE Trans. Circuits Syst.* **1995**, *42*, 864−872.

(9) Mutoh, S.; Douseki, T.; Matsuya, Y.; Aoki, T.; Shigematsu, S.; Yamada, J. 1-V power supply high-speed digital circuit technology with multithreshold-voltage. CMOS. *IEEE J. Solid-State Circuits* **1995**, *30*, 847−854.

(10) An, K.; Lee, H.-N.; Cho, K. H.; Lee, S.-W.; Hwang, D. J.; Kang, K.-T. Role of a 193 nm ArF excimer laser in laser-assisted plasma-enhanced chemical vapor deposition of SiNx for low temperature thin film encapsulation. *Micromachines* **2020**, *11*, No. 88.

(11) French, P.; Krijnen, G.; Roozeboom, F. Precision in harsh environments. *Microsyst. Nanoeng.* **2016**, *2*, No. 16048.

(12) Klauk, H.; Zschieschang, U.; Pflaum, J.; Halik, M. Ultralow-power organic complementary circuits. *Nature* **2007**, *445*, 745−748.

(13) Ma, P.; Du, L.; Wang, Y.; Jiang, R.; Xin, Q.; Li, Y.; Song, A. Low voltage operation of IGZO thin film transistors enabled by ultrathin Al2O3 gate dielectric. *Appl. Phys. Lett.* **2018**, *112*, No. 023501.

(14) Cai, W.; Park, S.; Zhang, J.; Wilson, J.; Li, Y.; Xin, Q.; Majewski, L.; Song, A. One-Volt IGZO thin-film transistors with ultra-thin solution-processed AlxOy gate dielectric. *IEEE Electron Device Lett.* **2018**, *39*, 375−378.

(15) Devi, D.; Rakesh, P.; Rakesh, V. Impact of scaling gate insulator thickness on the performance of carbon nanotube field effect transistors (CNTFETs). *J. Nano- Electron. Phys.* **2013**, *5*, No. 02014.

(16) Ding, X.; Zhang, J.; Shi, W.; Ding, H.; Zhang, H.; Li, J.; Jiang, X.; Zhang, Z.; Fu, C. Effect of gate insulator thickness on device performance of InGaZnO thin-film transistors. *Mater. Sci. Semicond. Process.* **2015**, *29*, 326−330.
(17) Kim, C. S.; Jo, S. J.; Lee, S. W.; Kim, W. J.; Baik, H. K.; Lee, S. J. Thickness dependence of gate dielectric layer on structural and electrical characteristics in the pentacene thin-film transistors. *J. Electrochem. Soc.* **2007**, *154*, H102−H104.
(18) Tate, J.; Rogers, J. A.; Jones, C. D.; Vyas, B.; Murphy, D. W.; Li, W.; Bao, Z.; Slusher, R. E.; Dodabalapur, A.; Katz, H. E. Anodization and microcontact printing on electroless silver: Solution-based fabrication procedures for low-voltage electronic systems with organic active components. *Langmuir* **2000**, *16*, 6054−6060.
(19) Iino, Y.; Inoue, Y.; Fujisaki, Y.; Fujikake, H.; Sato, H.; Kawakita, M.; Tokito, S.; Kikuchi, H. Organic thin-film transistors on a plastic substrate with anodically oxidized high-dielectric-constant insulators. *Jpn. J. Appl. Phys.* **2003**, *42*, 299−304.
(20) Majewski, L. A.; Grell, M.; Ogier, S. D.; Veres, J. A novel gate insulator for flexible electronics. *Org. Electron.* **2003**, *4*, 27−32.
(21) Majewski, L. A.; Schroeder, R.; Grell, M. Flexible high capacitance gate insulators for organic field effect transistors. *J. Phys. D: Appl. Phys.* **2004**, *37*, 21−24.
(22) Linfeng, L.; Junbiao, P. High-Performance Indium−Gallium−Zinc Oxide Thin-Film Transistors Based on Anodic Aluminum Oxide. *IEEE Trans. Electron Devices* **2011**, *58*, 1452−1455.
(23) Cai, W.; Wilson, J.; Zhang, J.; Park, S.; Majewski, L.; Song, A. Low-voltage, flexible InGaZnO thin-film transistors gated with solution-processed ultra-thin AlxOy. *IEEE Electron Device Lett.* **2018**, *40*, 36−39.
(24) Cai, W.; Zhang, J.; Wilson, J.; Song, A. Low-voltage, full-swing InGaZnO-based inverters enabled by solution-processed ultra-thin AlxOy. *IEEE Electron Device Lett.* **2019**, *40*, 1285−1288.
(25) Zhang, J.; Cai, W.; Wilson, J.; Ma, X.; Brownless, J.; Li, Y.; Yang, J.; Yuan, Y.; Ma, P.; Xin, Q. *Oxide Devices for Displays and Low Power Electronics*, Int. Symp. Dig. Tech. Pap. − International Conference on Display Technology; Suzhou, China; March 26−29, 2019; pp 81−84.
(26) Zhang, X.; Cai, W.; Zhang, J.; Brownless, J.; Wilson, J.; Zhang, Y.; Song, A. Solution-processed TiO2-based Schottky diodes with a large barrier height. *IEEE Electron Device Lett.* **2019**, *40*, 1378−1381.
(27) Cai, W.; Wilson, J.; Zhang, J.; Brownless, J.; Zhang, X.; Majewski, L. A.; Song, A. Significant performance enhancement of very thin InGaZnO thin-film transistors by a self-assembled monolayer treatment. *ACS Appl. Electron. Mater.* **2020**, *2*, 301−308.
(28) Shao, Y.; Xiao, X.; He, X.; Deng, W.; Zhang, S. Low-voltage a-InGaZnO thin-film transistors with anodized thin HfO2 gate dielectric. *IEEE Electron Device Lett.* **2015**, *36*, 573−575.
(29) Barquinha, P.; Vila, A. M.; Gonçalves, G.; Pereira, L.; Martins, R.; Morante, J. R.; Fortunato, E. Gallium−Indium−Zinc-Oxide-based thin-film transistors: Influence of the source/drain material. *IEEE Trans. Electron Devices* **2008**, *55*, 954−960.
(30) Yim, J.-R.; Jung, S.-Y.; Yeon, H.-W.; Kwon, J.-Y.; Lee, Y.-J.; Lee, J.-H.; Joo, Y.-C. Effects of metal electrode on the electrical performance of amorphous In−Ga−Zn−O thin film transistor. *Jpn. J. Appl. Phys.* **2011**, *51*, No. 011401.
(31) Li, Q.; Qiu, L.; Wei, X.; Dai, B.; Zeng, H. Point contact resistive switching memory based on self-formed interface of Al/ITO. *Sci. Rep.* **2016**, *6*, No. 29347.
(32) Zaffora, A.; Di Quarto, F.; Habazaki, H.; Valov, I.; Santamaria, M. Electrochemically prepared oxides for resistive switching memories. *Faraday Discuss.* **2019**, *213*, 165−181.
(33) Heljo, P. S.; Wolff, K.; Lahtonen, K.; Valden, M.; Berger, P. R.; Majumdar, H. S.; Lupo, D. Anodic oxidation of ultra-thin Ti layers on ITO substrates and their application in organic electronic memory elements. *Electrochim. Acta* **2014**, *137*, 91−98.
(34) Ip, K.; Heo, Y.; Baik, K.; Norton, D.; Pearton, S.; Ren, F. Specific contact resistance of Ti/Al/Pt/Au ohmic contacts to phosphorus-doped ZnO thin films. *J. Vac. Sci. Technol., B* **2004**, *22*, 171−174.
(35) Choi, S.-H.; Jung, W.-S.; Park, J.-H. Electrical effect of titanium diffusion on amorphous indium gallium zinc oxide. *Appl. Phys. Lett.* **2012**, *101*, No. 212105.
(36) Choi, K.-H.; Kim, H.-K. Correlation between Ti source/drain contact and performance of InGaZnO-based thin film transistors. *Appl. Phys. Lett.* **2013**, *102*, No. 052103.
(37) Eun Lee, J.; Sharma, B. K.; Lee, S.-K.; Jeon, H.; Hee Hong, B.; Lee, H.-J.; Ahn, J.-H. Thermal stability of metal ohmic contacts in indium gallium zinc oxide transistors using a graphene barrier layer. *Appl. Phys. Lett.* **2013**, *102*, No. 113112.
(38) Mudgal, T.; Walsh, N.; Manley, R. G.; Hirschman, K. D. Impact of annealing on contact formation and stability of IGZO TFTs. *ECS Trans.* **2014**, *61*, 405−417.
(39) Xu, L.; Huang, C.-W.; Abliz, A.; Hua, Y.; Liao, L.; Wu, W.-W.; Xiao, X.; Jiang, C.; Liu, W.; Li, J. The different roles of contact materials between oxidation interlayer and doping effect for high performance ZnO thin film transistors. *Appl. Phys. Lett.* **2015**, *106*, No. 051607.
(40) Hu, S.; Lu, K.; Ning, H.; Fang, Z.; Liu, X.; Xie, W.; Yao, R.; Zou, J.; Xu, M.; Peng, J. Effect of ITO serving as a barrier layer for Cu electrodes on performance of a-IGZO TFT. *IEEE Electron Device Lett.* **2018**, *39*, 504−507.
(41) Sharma, R.; Brendt, J.; Merkulov, A.; Wagner, V. Effects of post-lift-off annealing conditions on contact oxidation of Ti−Au top-contacts in In-Sn−Zn−O TFT. *Mater. Sci. Semicond. Process.* **2015**, *34*, 291−296.
(42) Nomura, K.; Kamiya, T.; Hosono, H. Effects of diffusion of hydrogen and oxygen on electrical properties of amorphous oxide semiconductor, In-Ga-Zn-O. *ECS J. Solid State Sci. Technol.* **2013**, *2*, P5−P8.
(43) Watanabe, K.; Lee, D.-H.; Sakaguchi, I.; Nomura, K.; Kamiya, T.; Haneda, H.; Hosono, H.; Ohashi, N. Surface reactivity and oxygen migration in amorphous indium-gallium-zinc oxide films annealed in humid atmosphere. *Appl. Phys. Lett.* **2013**, *103*, No. 201904.
(44) Prakash, G.; Gray, J. L.; Lee, Y. S.; Kanicki, J. Comparison of composition and atomic structure of amorphous indium gallium zinc oxide thin film transistor before and after positive bias temperature stress by transmission electron microscopy. *Semicond. Sci. Technol.* **2015**, *30*, No. 055008.
(45) Xiao, X.; Shao, Y.; He, X.; Deng, W.; Zhang, L.; Zhang, S. Back channel anodization amorphous Indium Gallium Zinc Oxide thin-film transistors process. *IEEE Electron Device Lett.* **2015**, *36*, 357−359.
(46) Dean, J. A. *Lange's Handbook of Chemistry*, 15th ed.; McGraw-Hill: New York, 1999.
(47) Yu, Y. Diffusion Reactions at Metal-oxide Interfaces and the Effect of an Applied Electric Field. Ph.D. Thesis, Case Western Reserve University: Cleveland, Ohio, 2005.
(48) Yao, M.; Chen, J.; Su, Z.; Peng, Y.; Li, F.; Yao, X. Ionic transport and barrier effect of anodic oxide layer in a solid-state Al2O3 capacitor under high electric field. *Electrochim. Acta* **2017**, *224*, 235−242.
(49) Jaju, V. Device Quality Low Temperature Gate Oxide Growth using Electron Cyclotron Resonance Plasma Oxidation of Silicon. Ph.D. Thesis, Iowa State University: Ames, Iowa, 2008.
(50) Li, F.; Jiang, X.; Shao, Z.; Zhu, D.; Luo, Z. Research progress regarding interfacial characteristics and the strengthening mechanisms of titanium alloy/hydroxyapatite composites. *Mater.* **2018**, *11*, No. 1391.
(51) Diggle, J. W.; Downie, T. C.; Goulding, C. Anodic oxide films on aluminum. *Chem. Rev.* **1969**, *69*, 365−405.
(52) Sowa, M.; Łastówka, D.; Kukharenko, A. I.; Korotin, D. M.; Kurmaev, E. Z.; Cholakh, S. O.; Simka, W. Characterisation of anodic oxide films on zirconium formed in sulphuric acid: XPS and corrosion resistance investigations. *J. Solid State Electrochem.* **2017**, *21*, 203−210.
(53) Ohgai, T. Magnetoresistance of Nanowires Electrodeposited into Anodized Aluminum Oxide Nanochannels. In *Nanowires-Recent Advances*, 1st ed.; Peng, X., Ed.; InTech: Croatia, 2012; pp 101−125.

https://dx.doi.org/10.1021/acsomega.0c04924
ACS Omega 2021, 6, 2717−2726

(54) Dey, A.; Singh, A.; Kalita, A.; Das, D.; Iyer, P. High performance low operating voltage n-Type organic field effect transistor based on inorganic-organic bilayer dielectric system. *J. Phys.: Conf. Ser.* **2016**, *704*, No. 01207.
(55) Du, X.; Xu, Y. Formation of Al2O3−BaTiO3 composite thin film to increase the specific capacitance of aluminum electrolytic capacitor. *Thin Solid Films* **2008**, *516*, 8436−8440.
(56) Kim, J. H.; Rim, Y. S.; Kim, H. J. Homojunction solution-processed metal oxide thin-film transistors using passivation-induced channel definition. *ACS Appl. Mater. Interfaces* **2014**, *6*, 4819−4822.

https://dx.doi.org/10.1021/acsomega.0c04924
ACS Omega 2021, 6, 2717−2726